ARTICLES

Reactions of Nitrogen Monoxide on Cobalt Cluster Ions: Reaction Enhancement by Introduction of Hydrogen

Tetsu Hanmura,[†] Masahiko Ichihashi,[‡] Yoshihide Watanabe,[§] Noritake Isomura,[§] and Tamotsu Kondow*[,‡]

East Tokyo Laboratory, Genesis Research Institute, Inc., 717-86 Futamata, Ichikawa, Chiba 272-0001, Japan, Cluster Research Laboratory, Toyota Technological Institute in East Tokyo Laboratory, Genesis Research Institute, Inc., 717-86 Futamata, Ichikawa, Chiba 272-0001, Japan, and Toyota Central R&D Labs., Inc., Nagakute, Aichi 480-1192, Japan

Received: May 27, 2006; In Final Form: September 19, 2006

Absolute cross sections for NO chemisorption, NO decomposition, and cluster dissociation in the collision of a nitrogen monoxide molecule, NO, with cluster ions Co_n^+ and Co_nH^+ ($n = 2-5$) were measured as a function of the cluster size, n, in a beam-gas geometry in a tandem mass spectrometer. Size dependency of the cross sections and the change of the cross sections by introduction of H to Co_n^+ (effect of H-introduction) are explained by a statistical model based on the RRK theory, with the aid of the energetics obtained by a DFT calculation. It was found that the reactions are governed by the energetics rather than dynamics. For instance, Co_3^+ does not react appreciably with NO because the reactions are endothermic, while Co_3H^+ does because the reaction becomes exothermic by the H-introduction.

1. Introduction

Size dependency of the reactivity of transition metal clusters in the gas phase has been studied extensively to find a correlation between the size dependency of the reactivity and the geometric and electronic structures of the clusters, such as correlation of size-dependent reaction cross sections with two-dimensional versus three-dimensional structures,[1] the ionization potential,[2,3] the HOMO−LUMO gap,[4,5] and the d-vacancies.[6] On the other hand, the geometric and electronic structures of a cluster are modified by introduction of foreign atoms into it. Among atoms used commonly, a hydrogen atom is of particular importance and vital utility because it is widely and abundantly distributed in nature. Actually, introduction of hydrogen atoms (H-introduction) causes the magnetic moments[7,8] of Fe_n^+ and Ni_n^+, the ionization potentials[9] of V_n, Nb_n, and Fe_n, the melting point[10] of Pd_n, and so forth, to change. It is expected as well that the reactivity changes with the H-introduction because the reactivity is influenced by change of the electronic structure. Several studies have been reported thus far on the effects of the H-introduction on the reactions involving metal cluster ions in the gas phase. Schnabel and Irion have revealed that the reaction rate of Fe_4^+ with ethane is diminished by the H-introduction, while that of Fe_3^+ with acetylene is elevated instead.[11] Vakhtin and Sugawara have found that the adsorption of one H_2 molecule on Nb_8^+ and Nb_{11}^+ increases the reactivity of the clusters toward another H_2 molecule.[12] On the other hand, Khairallah and O'Hair have observed that reactions of Ag_n^+ ($n = 3, 5, 7$) and $Ag_{n-1}H^+$ with 2-propanol and 2-butylamine do not change appreciably.[13]

It is widely recognized that catalytic removal of NO impurity from air becomes one of the most important environmental problems. Practical catalysts of NO removal consist of fine metal particles on substrates, and thus the size effect of the fine particles on the catalytic activity is of great importance. Klaassen and Jacobson[14,15] have studied reactions of $^{18}O_2$ and $H_2{}^{18}O$ with $Co_n(N^{16}O)^+$ ($n = 2-4$) and have concluded that NO is molecularly chemisorbed on Co_2^+ while it is dissociatively chemisorbed on $Co_{3,4}^+$. Castleman and co-workers[16] have studied reactions of NO with Ni_n^+ in a fast-flow reactor and have found that NO addition onto Ni_n^+ and oxidation of Ni_n^+ occur. Wu and Yang[17] have investigated reactions of Nb_n^+ with NO in a fast-flow reactor and have shown that dissociative chemisorption occurs dominantly for $n \leq 7$ while molecular adsorption occurs for $n \geq 8$. Mackenzie and co-workers[18,19] have observed reactions of $Rh_n^{+/-}$ by multiple collisions with NO molecules in FTICR and have shown that dissociative chemisorption of NO proceeds with rapid N_2 desorption in an early stage of the reactions.

It should be noted that the information obtained in the gas-phase reactions cannot be brought directly into the design of a corresponding heterogeneous catalytic reaction because the gas-phase reactions do not take the effect of the substrate of the catalyst into consideration. If one likes to design a practical cluster catalyst, it is necessary to consider how the reaction is influenced in the presence of the substrate. It has been reported that Au_8 catalyzes CO oxidation when it is placed on a defect-rich MgO(100) surface, whereas it does not catalyze significantly on a defect-free MgO(100) surface.[20] The reaction enhancement

* Corresponding author. Telephone: +81-47-320-5911. Fax: +81-47-327-8031. E-mail: kondow@clusterlab.jp.
[†] East Tokyo Laboratory, Genesis Research Institute, Inc.
[‡] Cluster Research Laboratory, Toyota Technological Institute in East Tokyo Laboratory, Genesis Research Institute, Inc.
[§] Toyota Central R&D Labs.

10.1021/jp063273a CCC: $37.00
Published on Web 12/30/2006

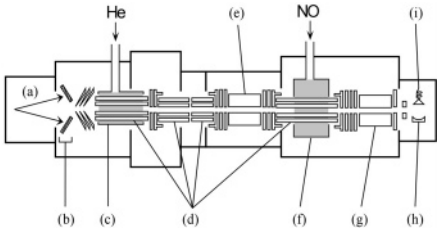

Figure 1. Schematic view of the apparatus. (a) Xenon (or argon) ion beam, (b) cobalt targets, (c) cooling cell, (d) octopole ion guides, (e) first quadrupole mass spectrometer, (f) reaction cell, (g) second quadrupole mass spectrometer, (h) ion conversion dynode, and (i) secondary electron multiplier.

by introducing defects on the surface is a typical example of the substrate effect and is attributed to partial electron transfer from the MgO surface to Au_8. The surface effect is also demonstrated computationally that the energy of CO chemisorption on Pt_2 increases by about 1 eV when it is placed on MgO(100) and BaO(100) surfaces.[21] In addition, even unintended surface species greatly change the reactivity. For instance, a trace amount of hydrogen introduced into a reaction system alters the rate and the selectivity of a catalyst.[22]

Under these circumstances, systematic investigation of NO reactions on metal cluster ions in the gas phase is of practical importance to design a practical cluster catalyst of NO removal with and without foreign atoms. In the present study, we investigated the influence of the size and the H-introduction on NO reactions on Co_n^+ by measuring absolute reaction cross sections of NO with Co_n^+ and Co_nH^+ ($n = 2-5$) as a function of the cluster size, n. Cobalt was chosen because (1) NO adsorption on a cobalt surface has attracted much attention[23,24] in connection with catalytic NO removal, and (2) cobalt consists of ^{59}Co with no other isotopic species, which facilitate mass spectroscopic selection of Co_n^+ and Co_nH^+ from a mixture of cobalt cluster ions produced in our cluster ion source.

2. Experimental Section

Figure 1 shows a schematic diagram of the apparatus. A brief description is given here since its detail has been reported.[25] The apparatus consists of a cluster ion source, a cooling cell, quadrupole mass spectrometers, a reaction cell, and a detector, which are connected by octopole ion guides for efficient transportation of ions. Parent cluster ions, Co_n^+ and Co_nH^+, were produced by sputtering four pieces of cobalt metals by rare gas (xenon or argon) ions with an acceleration energy up to 15 keV, where the rare gas ions were prepared in a plasma ion source (Rokion Ionenstahl-Technologie, CORDIS Ar25/35c). The hydrogenated cluster ions, Co_nH^+, were produced by reactions of cobalt cluster ions with residual impurities such as water present in the source. The cluster ions from the source were cooled in the cooling cell 290 mm in length and containing helium gas (pressure of $>10^{-3}$ Torr, temperature of $\sim$300 K) and then admitted into the first quadrupole mass spectrometer (Extrel, 162-8) for selection of cluster ions of a given size. The cluster ions size-selected in the mass spectrometer were admitted into an octopole ion guide surrounded by the reaction cell, in which the incoming cluster ions collide with nitrogen monoxide, NO, introduced through a variable leak valve (Granville-Phillips, series 203). A spinning rotor gauge (MKS, SRG-2) was used to measure the pressure in the reaction cell. To fulfill the single collision conditions, the pressure of the NO gas in the reaction cell was maintained at $\sim 5 \times 10^{-5}$ Torr. Product ions were mass analyzed in the second quadrupole mass spectrometer and detected by an ion conversion dynode followed by a secondary electron multiplier (Murata, Ceratron EMS-6081B) in a pulse counting mode. Signals from the secondary electron multiplier were processed in an electronic circuitry based on a personal computer.

The mass resolution of the first mass spectrometer was set to be sufficiently high to select a parent cluster ion of interest from other undesired ions,[26] while that of the second mass spectrometer was reduced to such an extent that the cross section for formation of a product ion can be determined reliably but the product ion is still identified confidently. The spread of the translational energy of parent cluster ions was measured to be typically 3 eV in the laboratory frame by applying a retarding voltage to the octopole ion guide in the reaction cell. This energy spread amounts to ± 0.2 eV in the center-of-mass frame in a collision involving a Co_3^+ ion.

A total reaction cross section (σ_r) for obtaining all the reaction product ions is given as

$$\sigma_r = \frac{k_B T}{Pl} \ln \frac{I + \sum I_p}{I} \quad (1)$$

where I and $\sum I_p$ represent the intensity of an intact parent ion passing through the collision region and the sum of the intensities of the product ions, respectively, P and T are the pressure and the temperature of the NO gas, respectively, l (= 120 mm) is the effective path length of the collision region, and k_B is the Boltzmann constant. A partial cross section (σ_p) for formation of a given product ion is expressed as

$$\sigma_p = \sigma_r \frac{I_p}{\sum I_p} \quad (2)$$

where $I_p/\sum I_p$ represents the branching fraction for a product ion of interest.

3. Computational Procedure

All the optimized geometries with given spin multiplicities were computed by a DFT method at a generalized gradient approximation (GGA) level in Amsterdam Density Functional (ADF) software package,[27] which is reported[28] to give a sufficiently accurate structure and a dissociation energy of Co_2. The triple-ζ basis sets extended with a polarization function were employed for all the atoms involved. The frozen core approximation was applied for the 1s−2p orbitals of a Co atom and the 1s orbital of the N and O atoms. The exchange-correlation terms adopted in the local density approximation were those of Vosko et al.[29] The exchange and the correlation functionals adopted for the GGA corrections were those of Becke[30] and Perdew,[31] respectively. The initial geometries of a species of interest were constructed by varying the interatomic distances and bond angles of the species having a reasonable structural symmetry. Different spin multiplicities were examined in all the calculations while taking the spin conservation into account (see section 4.2.A).

4. Results

4.1. Reaction Products and Cross Sections. Figure 2 shows typical mass spectra of ions obtained by the collision of NO with Co_3^+ (panel a) and with Co_3H^+ (panel b). In the collision of $Co_nH_m^+$ ($n = 2-5$, $m = 0$, 1) with NO, the ionic products are $Co_{n,n-1}H_mNO^+$, $Co_{n-1}N^+$, and Co_{n-1}^+. As described in section 5.1, processes of generating $Co_nH_mNO^+$ and $Co_{n-1}H_mNO^+$ are defined to be "NO chemisorption" because these ions are produced via chemisorption of NO on the parent cluster ions.

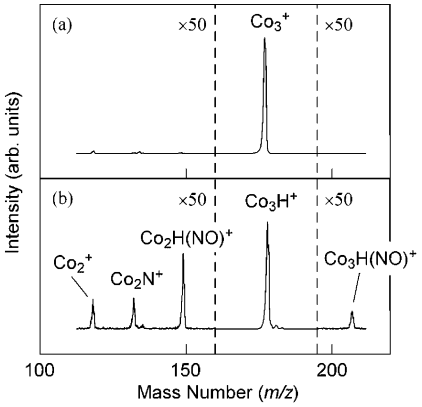

Figure 2. (a), (b) Mass spectra obtained in the collision of Co_3^+ and Co_3H^+ with NO, respectively, at the collision energy of 0.2 eV under the single collision condition. The peak assignments are illustrated in the spectra. Note that the signal intensity of the product ions is enlarged by 50 times.

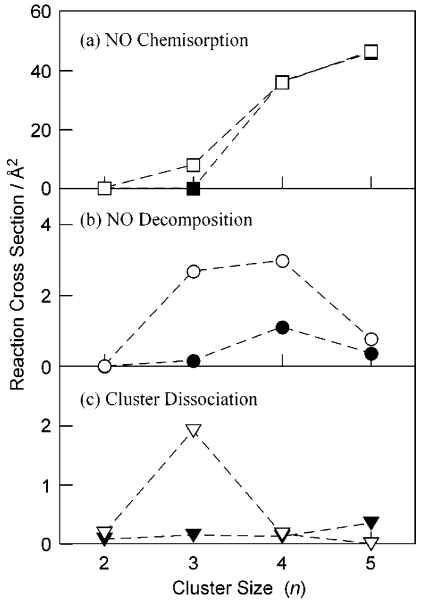

Figure 3. Reaction cross sections of NO chemisorption (a), NO decomposition (b), and cluster dissociation (c) of Co_n^+ (solid symbols) and Co_nH^+ (open symbols) at the collision energy of 0.2 eV. Note that, in several cases, the reaction cross sections for Co_n^+ and Co_nH^+ are so close that the solid symbols are hidden behind the open symbols.

Similarly, $Co_{n-1}N^+$ and Co_{n-1}^+ are produced via decomposition of NO and dissociation of the parent cluster ion, $Co_nH_m^+$, and hence defined to be "NO decomposition" and "cluster dissociation", respectively.

Figure 3 shows the cross sections of these reactions for Co_n^+ (solid symbols) and Co_nH^+ (open symbols) at the collision energy of 0.2 eV as a function of the cluster size, *n*. Note that, in several cases such as $n = 2$, 4, and 5 in panel a, the reaction cross sections for Co_n^+ and Co_nH^+ are so close that the solid symbols are hidden behind the open symbols. The absolute values of the cross sections are listed in Table 1. In the collision of Co_n^+ with NO, the cross section for the NO chemisorption (■ in panel a) increases steeply at $n = 4$ with the cluster size, while those for the NO decomposition (● in panel b) and the cluster dissociation (▲ in panel c) are extremely small and almost independent of the size. In the collision of Co_3H^+, the cross sections for the NO chemisorption, the NO decomposition, and the cluster dissociation (□, O, and △ in panels a, b, and c, respectively) are larger than those of Co_3^+. Namely, these reaction cross sections increase by introduction of one hydrogen atom (H-introduction) to Co_3^+. The cross section for the NO decomposition is also enhanced at $n = 4$ by the H-introduction.

TABLE 1: Reaction Cross Sections (Å²) Measured at the Collision Energy of 0.2 eV

	NO chemisorption		NO decomposition		NO dissociation	
n	Co_n^+	Co_nH^+	Co_n^+	Co_nH^+	Co_n^+	Co_nH^+
2	0.3	0.3	0.0	0.0	0.1	0.2
3	0.1	8.1	0.2	2.7	0.1	1.9
4	36.3	35.9	1.1	3.0	0.1	0.2
5	45.9	46.5	0.4	0.8	0.3	0.0

4.2. Structures and Energies of Parent, Intermediate, and Product Species. *4.2.A. Restriction by Spin Conservation.* The structures and the energies of parent ions, $Co_nH_m^+$ ($n = 2$, 3; $m = 0$, 1), were obtained by the calculation mentioned in section 3. The structure having the lowest energy among the energy minimum structures with all the possible spin multiplicities was determined to be the structure for the parent cluster ion in the electronic ground state (see section 4.2.B).

In the calculation of reaction intermediates and product ions, their spin multiplicities were determined from those of the corresponding parent cluster ions (M_{par}) by taking advantage of the spin conservation rule that holds in a reaction consisting of atoms having weak spin−orbit interaction. The initial geometries of reaction intermediates, $Co_nH_m(NO)^+$ and $Co_nH_m(N)(O)^+$, having the spin multiplicities of $M_{par} \pm 1$ were constructed, and the actual geometries and the energies of the reaction intermediates having the spin multiplicity of M_{int} were obtained by the geometry optimization described in section 3. Similar calculations were performed on the product ions (M_{ion}) and the counter neutrals (M_{neu}) by considering the spin conservation relation ($|S_{ion} - S_{neu}| \le S_{int} \le S_{ion} + S_{neu}$ with $M = 2S + 1$).

4.2.B. Optimized Structures and Energies. Figure 4 shows the optimized geometries, the energies, and the spin multiplicities of the parent cluster ions at $n = 2$, 3 and their product ions, where the energy values shown are evaluated with respect to the initial reaction channel ($Co_nH_m^+ + NO$).

The parent cluster ions, Co_2^+ (geometry a), Co_2H^+ (geometry b), and Co_3^+ (geometry c), in the ground state have the spin multiplicities of $M_{par} = 6$, 5, and 7, respectively. On the other hand, Co_3H^+ with $M_{par} = 8$ has the lowest energy but lower only by 0.02 eV than that with $M_{par} = 6$ (geometry d), and therefore the reaction intermediates from both $M_{par} = 6$ and 8 were calculated for the Co_3H^+ reactions. The bond lengths were obtained as 2.01 Å for linear Co_2^+ and 2.13−2.23 Å for Co_3^+ in an isosceles triangle form. The H atom in both Co_2H^+ and Co_3H^+ is located at the bridge site between two Co atoms. The bond length of Co_2^+ in the ground state given by the present calculation agrees well with the value of 2.09−2.11 Å[32] and 1.94−1.96 Å[33] obtained by other groups.

In the reaction intermediates of a molecularly chemisorbed type, $Co_2(NO)^+$, $Co_2H(NO)^+$, $Co_3(NO)^+$, and $Co_3H(NO)^+$ owning the spin multiplicities of $M_{int} = 5$, 4, 6, and 5, respectively, were found to have the lowest energies among the geometries examined. The optimized geometries of the intermediates of a dissociatively chemisorbed type, $Co_2(N)(O)^+$, $Co_2H(N)(O)^+$, $Co_3(N)(O)^+$, and $Co_3H(N)(O)^+$ owning the spin multiplicities of $M_{int} = 5$, 4, 6, and 5, respectively, were also obtained. Finally, in the product ions (the spin multiplicities of M_{ion}) and the counter neutrals (the spin multiplicities of M_{neu}), geometries e−g, h−j, k−m, and n−p in Figure 4 were found to have the lowest energies among the species obtained from

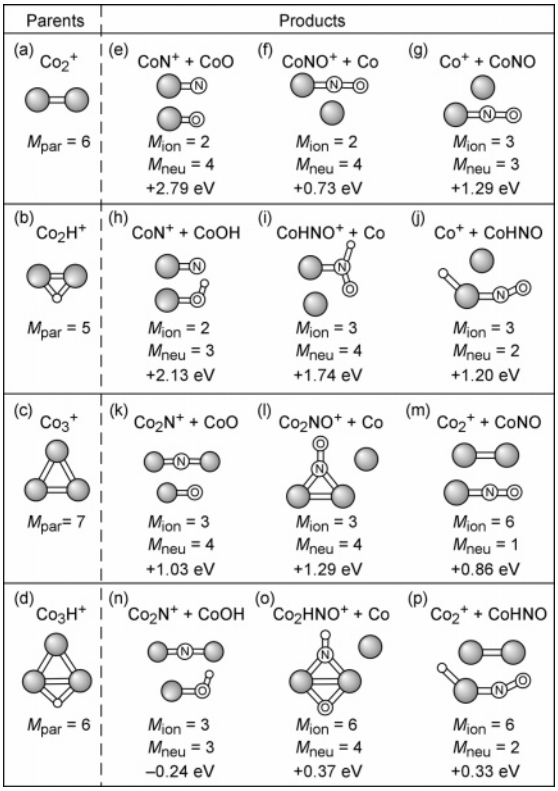

Figure 4. Optimized geometries of the parent cluster ions and the product species emerging in the reactions involving Co_2^+, Co_2H^+, Co_3^+, and Co_3H^+, together with the energy and the spin multiplicity, *M*; geometries (a−d) are the parent cluster ions and geometries (e−p) are the product species. The energies are shown with respect to the entrance channel of the reaction, $Co_nH_m^+ + NO$.

the reactions of NO with Co_2^+, Co_2H^+, Co_3^+, and Co_3H^+, respectively. Note that Co_2NO^+ in the ground state having $M_{ion} = 3$ (see geometry l), in which the molecularly adsorbed NO is bound to the Co−Co axis perpendicularly, has a structure similar to that obtained by another group;[34] the bond lengths obtained by these calculations agree within 0.05 Å.

5. Discussion

5.1. Reaction Processes. The experimental and computational results given in sections 4.1 and 4.2 are explained by assuming that the following reaction processes take place: an incoming NO molecule is chemisorbed by a parent cluster ion, $Co_nH_m^+$, molecularly and dissociatively as

$$Co_nH_m^+ + NO \rightarrow Co_nH_m(NO)^+ \quad (3)$$

$$Co_nH_m(NO)^+ \rightarrow Co_nH_m(N)(O)^+ \quad (4)$$

The molecularly chemisorbed intermediate, $Co_nH_m(NO)^+$, is stabilized with releasing one Co atom as

$$Co_nH_m(NO)^+ \rightarrow Co_{n-1}H_m(NO)^+ + Co \quad (5)$$

or with releasing $CoH_m(NO)$ as

$$Co_nH_m(NO)^+ \rightarrow Co_{n-1}^+ + CoH_m(NO) \quad (6)$$

Reactions 5 and 6 are defined here to be the NO chemisorption and the cluster dissociation, respectively. On the other hand, the dissociatively chemisorbed intermediate, $Co_nH_m(N)(O)^+$, is stabilized with releasing Co into $Co_{n-1}H_m(N)(O)^+$ or releasing $CoOH_m$ into $Co_{n-1}N^+$ as

$$Co_nH_m(N)(O)^+ \rightarrow Co_{n-1}H_m(N)(O)^+ + Co \quad (7)$$

$$Co_nH_m(N)(O)^+ \rightarrow Co_{n-1}N^+ + CoOH_m \quad (8)$$

Reactions 7 and 8 are defined here to be the NO dissociative chemisorption and the NO decomposition, respectively. The present experiments cannot clarify whether NO is molecularly or dissociatively chemisorbed on Co_nH_m, but the calculations can (see section 4.2).

5.2. Reaction Scheme and Kinetic Model of Co_3H^+ Reaction. The reactions involving Co_3H^+ are analyzed in detail as a typical example that represents the reaction scheme of all the parent cluster ions studied. This reaction is scrutinized in particular, since the NO reaction on Co_3^+ is significantly influenced by the introduction of a hydrogen atom to it. Let us imagine that an incoming NO molecule having an induced dipole moment is captured by the positive charge of the parent cluster ion, Co_3H^+. The NO molecule, which is weakly captured as $Co_3H^+\cdots NO$, turns out to be chemisorbed on the parent cluster ion into $Co_3H(NO)^+$ (molecularly chemisorbed) or into $Co_3H(N)(O)^+$ (dissociatively chemisorbed) or is detached from it. Finally, the chemisorbed reaction intermediate dissociates into the product ions. The capture cross section is approximated by the Langevin cross section[35] in which one considers only a charge-induced dipole interaction. Even though a charge-permanent dipole interaction is included on the basis of ADO theory,[36,37] the cross section increases only by 1%. Therefore, the Langevin cross section was used here without taking the permanent dipole of NO into account. The rate constants of the chemisorption and the dissociation are given by the RRK theory.[38,39] It is reasonable to apply the RRK theory to evaluate the reaction rates because a sizable number of atoms are involved in the reactions together with slow collision between the NO molecule and the parent cluster ion.

All the reaction steps of the NO decomposition from $Co_3H^+\cdots NO$ are expressed as follows. The corresponding potential energy curve is shown in Figure 5a, where the reaction intermediates are denoted as **A**, **C**, and **E**.

$$Co_3H^+ + NO \overset{k_0}{\leftarrow} Co_3H^+\cdots NO \quad \text{(NO detachment)} \quad (9)$$

$$Co_3H^+\cdots NO \overset{k_1}{\rightarrow} Co_3H(NO)^+ \quad \text{(formation of A)} \quad (10)$$

$$Co_3H^+\cdots NO \overset{k_2}{\leftarrow} Co_3H(NO)^+ \quad (11)$$

$$Co_3H(NO)^+ \overset{k_3}{\rightarrow} Co_3(H)(N)(O)^+ \quad \text{(transition from A to C)} \quad (12)$$

$$Co_3H(NO)^+ \overset{k_4}{\leftarrow} Co_3(H)(N)(O)^+ \quad (13)$$

$$Co_3(H)(N)(O)^+ \overset{k_5}{\rightarrow} Co_3(N)(OH)^+ \quad \text{(transition from C to E)} \quad (14)$$

$$Co_3(H)(N)(O)^+ \overset{k_6}{\leftarrow} Co_3(N)(OH)^+ \quad (15)$$

$$Co_3(N)(OH)^+ \overset{k_7}{\rightarrow} Co_2N^+ + CoOH \quad \text{(NO decomposition)} \quad (16)$$

where k represents the rate constant of a given reaction step. On the other hand, all the reaction steps of the NO chemisorption and the cluster dissociation are given as follows, where the steps before the molecular chemisorption (formation of **A**) are not shown because they are identical to those given above (see also the potential curves shown in Figure 5b, where the reaction intermediates are denoted as **A**, **G**, and **I**):

$$Co_3H(NO)^+ \xrightarrow{k_8} Co_3(H)(N)(O)^+ \quad \text{(transition from A to G)} \tag{17}$$

$$Co_3H(NO)^+ \xleftarrow{k_9} Co_3(H)(N)(O)^+ \tag{18}$$

$$Co_3(H)(N)(O)^+ \xrightarrow{k_{10}} Co_3(O)(NH)^+ \quad \text{(transition from G to I)} \tag{19}$$

$$Co_3(H)(N)(O)^+ \xleftarrow{k_{11}} Co_3(O)(NH)^+ \tag{20}$$

$$Co_3(O)(NH)^+ \xrightarrow{k_{12}} Co_2(O)(NH)^+ + Co \quad \text{(NO chemisorption)} \tag{21}$$

$$Co_3H(NO)^+ \xrightarrow{k_{13}} Co_2^+ + CoHNO \quad \text{(cluster dissociation)} \tag{22}$$

The corresponding rate equations based on all these reaction steps of the NO decomposition are given as

$$\frac{d[Co_3H^+\cdots NO]}{dt} = -(k_0 + k_1)[Co_3H^+\cdots NO] + k_2[Co_3H(NO)^+] \tag{23}$$

$$\frac{d[Co_3H(NO)^+]}{dt} = k_1[Co_3H^+\cdots NO] - (k_2 + k_3 + k_8)[Co_3H(NO)^+] + k_4[Co_3(H)(N)(O)^+] + k_9[Co_3(H)(N)(O)^+] \tag{24}$$

$$\frac{d[Co_3(H)(N)(O)^+]}{dt} = k_3[Co_3H(NO)^+] - (k_4 + k_5)[Co_3(H)(N)(O)^+] + k_6[Co_3(N)(OH)^+] \tag{25}$$

$$\frac{d[Co_3(N)(OH)^+]}{dt} = k_5[Co_3(H)(N)(O)^+] - (k_6 + k_7)[Co_3(N)(OH)^+] \tag{26}$$

$$\frac{d[Co_2N^+]}{dt} = k_7[Co_3(N)(OH)^+] \tag{27}$$

where [X] represents the abundance of X. The rate equations of the NO chemisorption and the cluster dissociation were constructed in a similar manner.

The abundance of any species, X, at the reaction time, t, is numerically calculated by using the following equation:

$$[X]\,(t = t_{i+1}) = [X]\,(t = t_i) + \frac{d[X]}{dt}(t = t_i) \times \Delta t \tag{28}$$

In the present analysis, the time step, Δt, and the total reaction time were set to be 0.1 ps and ~100 μs (the flight time of species X between the center of the reaction cell and the entrance of the second mass spectrometer), respectively. The RRK theory gives the rate constant, k_j, as

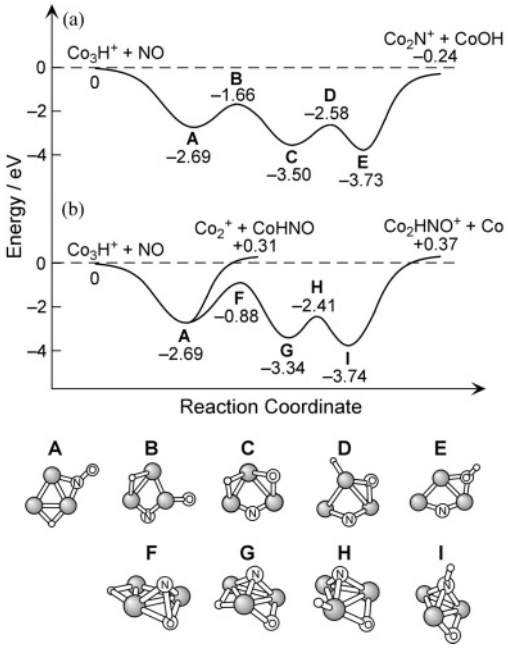

Figure 5. Potential energy curve for the NO decomposition (a) and the NO chemisorption and the cluster dissociation (b) on Co_3H^+. The numbers shows the energies of the reaction intermediate, transition, and product states in electronvolts with respect to the energy of the entrance channel, $Co_3H^+ + NO$. The optimized structures of the reaction intermediates (**A**, **C**, **E**, **G**, and **I**) and the transition state species (**B**, **D**, **F**, and **H**) are illustrated.

$$k_j = A_j\left(\frac{E_{int} + E_{col} + E_{Bj} - E_{A_j}}{E_{int} + E_{col} + E_{B_j}}\right)^{N-1} \tag{29}$$

where A_j is the prefactor along the reaction coordinate, E_{int} is the internal energy of the parent cluster ion and the NO molecule before the collision, E_{col} is the collision energy, E_{B_j} is the energy of the j-th species with respect to that of the initial state ($Co_3H^+ + NO$), E_{A_j} is the activation energy along the reaction coordinate, and N is the number of the vibrational modes of $Co_3H(NO)^+$. The prefactor, A_j, is assumed to be the vibrational frequency related to the reaction coordinate concerned; the prefactors employed in this analysis are the vibrational frequency of N−O of a NO adsorbate on a cobalt surface,[24] that of Co−N in a cobalt complex,[40] that of Co−O of an atomic oxygen adsorbed on a cobalt surface,[41] and that of a Co−Co bond of Co_3 estimated by Jarrold and Bower's method.[42] The partial reaction cross section, σ_i, for the production of X_i is given by

$$\sigma_i = \sigma_L \times \frac{[X_i]}{\sum_j [X_j]} \tag{30}$$

where σ_L is the Langevin cross section, which is calculated to be 49.3 Å^2 at $E_{col} = 0.2$ eV.

The cross sections for the NO chemisorption, the NO decomposition, and the cluster dissociation were calculated by solving the rate equations together with the Langevin cross section. In this calculation, the energies of the reaction intermediate and the transition states were obtained from the DFT calculation (see the schematic reaction potentials in Figure 5); the reaction intermediates are $Co_3H(NO)^+$ (**A**), $Co_3(H)(N)$-

$(O)^+$ (**C** and **G**), $Co_3(N)(OH)^+$ (**E**), and $Co_3(O)(NH)^+$ (**I**), while the transition state species were obtained as **B**, **D**, **F**, and **H** in Figure 5.

The calculation based on the model described above gives the cross sections of 3.8, 5.6, and ~0 Å^2 for the NO decomposition, the NO chemisorption, and the cluster dissociation, respectively, at the collision energy of 0.2 eV and they are compared with the experimental cross sections of 2.7, 8.1, and 1.9 Å^2. It is obvious that the calculation reproduces the NO chemisorption and the NO decomposition but does not for the cluster dissociation. In the framework of the present model, the disagreement between measured and calculated cross sections of the cluster dissociation arises because the energy level of $Co_2^+ + CoHNO$ is overestimated. It was found from several test calculations that a slight variation in the energy level of the product species largely affects the reaction rate calculated by RRK theory, while the vibrational frequency and the energy levels of the intermediate species are less effective, which is consistent with the report by Jarrold and Bowers.[42]

On the other hand, the cross sections for all three reactions on Co_3^+ are estimated to be zero by the present model because these reactions are endothermic at about 1 eV and the energy barrier cannot be surmounted under the present experimental condition with the collision energy of 0.2 eV and the internal energy of about 0.2 eV at 300 K; the reaction rate calculated by RRK theory turns out to be zero when the energy barrier is not surmounted. Thus, the present model based on the energetics reproduces the increase of the reaction cross sections by the H-introduction into Co_3^+.

5.3. Chemisorption Cross Sections versus Bond Energies. The size dependency of the NO chemisorption cross section on Co_n^+ and Co_nH^+ is explained in terms of the energetics by employing the model mentioned above. As shown in Figure 3, the cross sections of the NO chemisorption on Co_n^+ and Co_nH^+ are comparable to the Langevin cross section at $n = 4, 5$, while they are much smaller at $n = 2, 3$. In the NO chemisorption, the exit channels involve breaking either the $Co_nH_m^+-(NO)$ bond or the $Co_{n-1}H_mNO^+-Co$ bond. In the present statistical model, one exit channel is more favored if it has a lower energy. The calculation shows that the energy for breaking the $Co_{n-1}H_mNO^+-Co$ bond is larger than that needed to break the $Co_nH_m^+-(NO)$ bond at $n = 2, 3$, and hence the NO chemisorption (breaking of the $Co_{n-1}H_mNO^+-Co$ bond) does not occur efficiently at $n = 2, 3$. In fact, this theoretical prediction is consistent with the experimental result that the cross sections for the NO chemisorption are extremely small at $n = 2, 3$. The large cross sections for the NO chemisorption at $n = 4, 5$ lead us to conclude that the energy for breaking the $Co_nH_m^+-(NO)$ bond is larger than that for breaking the $Co_{n-1}H_mNO^+-Co$ bond if the present model is valid.

5.4. Reaction Enhancement by Introduction of Hydrogen Atom. The cross sections for the reactions involving Co_3^+ are found to be increased by the introduction of a hydrogen atom. The increment of the cross sections by the H-introduction can be explained by the energetics of the reactions in the RRK framework if the energy barriers among the reaction intermediates are lower than the energies of the product channels. In fact, in the reactions involving $Co_{2,3}^+$ and $Co_{2,3}H^+$, the energies of the product channels are shown by the present calculation to be higher than the barrier heights. As described in the following paragraph, the trimer ion, Co_3^+, does not react appreciably with NO because the reactions are endothermic, while Co_3H^+ does (increment of the cross sections) because the reactions become exothermic.

Let us explain the increment of the reaction cross sections by taking advantage of the energetics obtained computationally. In the reactions of Co_3^+, the NO chemisorption, the NO decomposition, and the cluster dissociation are endothermic by 1.03, 1.29, and 0.86 eV, respectively (see geometries k−m in Figure 4). This is consistent with the experimental result that the reaction cross sections of Co_3^+ are extremely small. In the reactions of Co_3H^+, the NO decomposition is exothermic by 0.24 eV, while the NO chemisorption and the cluster dissociation are endothermic by 0.37 and 0.33 eV, respectively (see geometries n−p in Figure 4). Although both the NO chemisorption and the cluster dissociation are endothermic, these reactions proceed because the reactants have a sizable amount of internal and collision energies. The energetics changes by the H-introduction probably because −OH and −NH groups are formed by the H-introduction and as a result the product states are stabilized. Namely, the binding energies of the N−H and O−H bonds are significantly larger than that of the Co−H bond; for instance, the binding energies of NH and OH molecules are 3.51 and 4.43 eV, respectively,[43] while the energy for chemisorption of an atomic hydrogen on a Co(0001) surface (the energy of a Co−H bond) is 2.60 eV.[44]

On the other hand, a NO molecule reacts with neither Co_2^+ nor Co_2H^+ because these reactions are significantly endothermic (see geometries e−g and h−j in Figure 4), although the present DFT calculation found that the dissociatively chemisorbed intermediates and the products are also energetically stabilized by the H-introduction at $n = 2$ when the −NH or the −OH group is formed. In other words, the energies of the dissociatively chemisorbed intermediates and the products relative to that of the initial state are too high at $n = 2$ even after the H-introduction. This difference in energetics between $n = 2$ and 3 could originate from the difference in geometry. In the dissociatively chemisorbed intermediate of $n = 2$, both the N and O atoms are located on the bridge site of the same pair of the two Co atoms. On the other hand, in the dissociative chemisorbed intermediates of $n = 3$, the N and O atoms are located on bridge sites of different sides of the triangle formed by the three Co atoms. It seems that the dissociatively chemisorbed intermediate of $n = 2$ is less stable than that of $n = 3$ because of the steric repulsion resulting from the fact that the N and O atoms are located so close on the cluster.

6. Conclusions

The present study showed that the NO chemisorption, the NO decomposition, and the cluster dissociation take place in the collision of a NO molecule with a cobalt cluster ion and are significantly influenced by the introduction of a hydrogen atom to the cluster ion. The size dependency and the effect of the H-introduction are interpreted in the RRK framework by taking advantage of the energetics of the reactions obtained by the DFT calculation. The effect of the H-introduction obtained in the present study corresponds to the effect of the hydrogen introduction in heterogeneous catalysts.

Acknowledgment. This work was supported by the Special Cluster Research Project of Genesis Research Institute, Inc.

References and Notes

(1) Ichihashi, M.; Corbett, C. A.; Hanmura, T.; Lisy, J. M.; Kondow, T. *J. Phys. Chem. A* **2005**, *109*, 7872.

(2) Whetten, R. L.; Cox, D. M.; Trevor, D. J.; Kaldor, A. *Phys. Rev. Lett.* **1985**, *54*, 1494.

(3) Whetten, R. L.; Zakin, M. R.; Cox, D. M.; Trevor, D. J.; Kaldor, A. *J. Chem. Phys.* **1986**, *85*, 1697.

(4) Conceicao, J.; Laaksonen, R. T.; Wang, L.-S.; Guo, T.; Nordlander, P.; Smalley, R. E. *Phys. Rev. B* **1995**, *51*, 4668.
(5) Kietzmann, H.; Morenzin, J.; Bechthold, P. S.; Ganteför, G.; Eberhardt, W. *J. Chem. Phys.* **1998**, *109*, 2275.
(6) Yadav, R. T.; Ichihashi, M.; Kondow, T. *J. Phys. Chem. A* **2004**, *108*, 7188.
(7) Knickelbein, M. B. *Chem. Phys. Lett.* **2002**, *353*, 221.
(8) Knickelbein, M. B. *J. Chem. Phys.* **2002**, *116*, 9703.
(9) Zakin, M. R.; Cox, D. M.; Whetten, R. L.; Trevor, D. J.; Kaldor, A. *Chem. Phys. Lett.* **1987**, *135*, 223.
(10) Grönbeck, H.; Tománek, D.; Kim, S. G.; Rosén, A. *Z. Phys. D* **1997**, *40*, 469.
(11) Schnabel, P.; Irion, M. P. *Ber. Bunsen-Ges. Phys. Chem.* **1992**, *96*, 1101.
(12) Vakhtin, A. B.; Sugawara, K. *Chem. Phys. Lett.* **1999**, *299*, 553.
(13) Khairallah, G. N.; O'Hair, R. A. J. *Dalton Trans.* **2005**, 2702.
(14) Klaassen, J. J.; Jacobson, D. B. *J. Am. Chem. Soc.* **1988**, *110*, 974.
(15) Klaassen, J. J.; Jacobson, D. B. *Inorg. Chem.* **1989**, *28*, 2022.
(16) Vann, W. D.; Bell, R. C.; Castleman, A. W., Jr. *J. Phys. Chem. A* **1999**, *103*, 10846.
(17) Wu, Q.; Yang, S. *Int. J. Mass Spectrom.* **1999**, *184*, 57.
(18) Ford, M. S.; Anderson, M. L.; Barrow, M. P.; Woodruff, D. P.; Drewello, T.; Derrick, P. J.; Mackenzie, S. R. *Phys. Chem. Chem. Phys.* **2005**, *7*, 975.
(19) Anderson, M. L.; Ford, M. S.; Derrick, P. J.; Drewello, T.; Woodruff, D. P.; Mackenzie, S. R. *J. Phys. Chem. A* **2006**, *110*, 10992.
(20) Sanchez, A.; Abbet, S.; Heiz, U.; Schneider, W.-D.; Häkkinen, H.; Barnett, R. N.; Landman, U. *J. Phys. Chem. A* **1999**, *103*, 9573.
(21) Grönbeck, H.; Broqvist, P. *J. Chem. Phys.* **2003**, *119*, 3896.
(22) Paal, Z.; Menon, P. G. *Catal. Rev.—Sci. Eng.* **1983**, *25*, 229.
(23) Bridge, M. E.; Lambert, R. M. *Surf. Sci.* **1980**, *94*, 469.
(24) Gu, J.; Yeo, Y. Y.; Mao, L.; King, D. A. *Surf. Sci.* **2000**, *464*, 68.
(25) Ichihashi, M.; Hanmura, T.; Yadav, R. T.; Kondow, T. *J. Phys. Chem. A* **2000**, *104*, 11885.
(26) Hanmura, T.; Ichihashi, M.; Monoi, T.; Matsuura, K.; Kondow, T. *J. Phys. Chem. A* **2004**, *108*, 10434.
(27) (a) *ADF 2003.01*; SCM, Theoretical Chemistry, Vrije Universiteit: Amsterdam, The Netherlands. http://www.scm.com. (b) te Velde, G.; Bickelhaupt, F. M.; Baerends, E. J.; Fonseca Guerra, C.; van Gisbergen, S. J. A.; Snijders, J. G.; Ziegler, T. *J. Comput. Chem.* **2001**, *22*, 931. (c) Fonseca Guerra, C.; Snijders, J. G.; te Velde, G.; Baerends, E. J. *Theor. Chem. Acc.* **1998**, *99*, 391.
(28) Wang, X.; Cao, Z.; Lu, X.; Lin, M.; Zhang, Q. *J. Chem. Phys.* **2005**, *123*, 064315.
(29) Vosko, S. H.; Wilk, L.; Nusair, M. *Can. J. Phys.* **1980**, *58*, 1200.
(30) Becke, A. D. *Phys. Rev. A* **1988**, *38*, 3098.
(31) Perdew, J. P. *Phys. Rev. B* **1986**, *33*, 8822.
(32) Gutsev, G. L.; Bauschlicher, C. W., Jr. *J. Phys. Chem. A* **2003**, *107*, 4755.
(33) Jamorski, C.; Martinez, A.; Castro, M.; Salahub, D. R. *Phys. Rev. B* **1997**, *55*, 10905.
(34) Martinez, A.; Jamorski, C.; Medina, G.; Salahub, D. R. *J. Phys. Chem. A* **1998**, *102*, 4643.
(35) Levine, R. D.; Bernstein, R. B. *Molecular Reaction Dynamics*; Oxford University Press: Oxford, 1974.
(36) Su, T.; Bowers, M. T. *J. Chem. Phys.* **1973**, *58*, 3027.
(37) Bass, L.; Su, T.; Chesnavich, W. J.; Bowers, M. T. *Chem. Phys. Lett.* **1975**, *34*, 119.
(38) Rice, O. K.; Ramsperger, H. C. *J. Am. Chem. Soc.* **1927**, *49*, 1617.
(39) Kassel, L. S. *J. Phys. Chem.* **1928**, *32*, 225.
(40) Durig, J. R.; Wertz, D. W. *Appl. Spectrosc.* **1968**, *22*, 627.
(41) Geerlings, J. J. C.; Zonnevylle, M. C.; de Groot, C. P. M. *Surf. Sci.* **1991**, *241*, 315.
(42) Jarrold, M. F.; Bower, J. E. *J. Chem. Phys.* **1987**, *87*, 5728.
(43) Lide, D. R. *CRC Handbook of Chemistry and Physics*, 78th ed.; CRC Press: Boca Raton, FL, 1997.
(44) Christmann, K. *Surf. Sci. Rep.* **1988**, *9*, 1.